J. Fluid Mech. (1988), *vol.* 189, *pp.* 165–187
Printed in Great Britain

Numerical models and experiments on immiscible displacements in porous media

By ROLAND LENORMAND, ERIC TOUBOUL
Dowell Schlumberger, B.P. 90, 42003 Saint Etienne Cedex 1, France

AND CESAR ZARCONE
Institut de Mécanique des Fluides, 2 rue C. Camichel, 31071 Toulouse Cedex, France.

(Received 30 June 1987)

Immiscible displacements in porous media with both capillary and viscous effects can be characterized by two dimensionless numbers, the capillary number C, which is the ratio of viscous forces to capillary forces, and the ratio M of the two viscosities. For certain values of these numbers, either viscous or capillary forces dominate and displacement takes one of the basic forms: (*a*) viscous fingering, (*b*) capillary fingering or (*c*) stable displacement. We present a study in the simple case of injection of a non-wetting fluid into a two-dimensional porous medium made of interconnected capillaries. The first part of this paper presents the results of network simulators (100×100 and 25×25 pores) based on the physical rules of the displacement at the pore scale. The second part describes a series of experiments performed in transparent etched networks. Both the computer simulations and the experiments cover a range of several decades in C and M. They clearly show the existence of the three basic domains (capillary fingering, viscous fingering and stable displacement) within which the patterns remain unchanged. The domains of validity of the three different basic mechanisms are mapped onto the plane with axes C and M, and this mapping represents the 'phase-diagram' for drainage. In the final section we present three statistical models (percolation, diffusion-limited aggregation (DLA) and anti-DLA) which can be used for describing the three 'basic' domains of the phase-diagram.

1. Introduction

Immiscible displacement in porous media is still the subject of active research, both theoretical and experimental. Although the physical mechanisms at the pore scale seem to be understood and are much easier to model than in the case of miscible fluids, the macroscopic description of the displacement remains a problem when fingering occurs on a large scale.

The long-term purpose of our study is to determine the saturation, the finger length and the size of the trapped clusters as functions of the geometry of the medium and the flow conditions. Our approach is based on the notion of 'phase-diagram' proposed in a short note by Lenormand (1985). Fluid displacement can be characterized by two dimensionless numbers; the capillary number C, which is the ratio of viscous forces to capillary forces, and the ratio M of the two viscosities. For certain values of these numbers, either viscous or capillary forces dominate and displacement takes one of the basic forms: (*a*) viscous fingering, (*b*) capillary fingering or (*c*) stable displacement. The domains of validity of the different basic

mechanisms can be mapped onto the plane with axes C and M. This mapping has been called the 'phase-diagram' for immiscible displacements.

The main purpose of this paper is the verification of this notion of phase-diagram in the very simple case of a two-dimensional porous medium made of interconnected capillaries. The first part of this paper presents the results of a network simulator based on the *physical* rules of the displacement at the pore scale. The second part describes a series of experiments in transparent etched networks. Both the computer simulations and the experiments clearly show the existence of the three domains within which the patterns remain unchanged, and the corresponding values of M and C are in good agreement. In the final section we present three *statistical* models (percolation, diffusion-limited aggregation (DLA) and anti-DLA) which describe the 'basic' domains of the phase-diagram.

2. The physical network simulator

The objective of our network simulator is to reproduce the behaviour of a large network of pores and throats (assumed to represent the porous sample) from the combination of physical laws governing the mechanisms at the pore level. The study will be illustrated in the particular case of a two-dimensional square network; this both simplifies the computer simulations and allows a direct comparison of the simulations with experiments performed in micromodels.

2.1. *Principle of the network simulator*

The idea of modelling a porous medium by a network of randomly sized pores joined by randomly sized throats has been used by several authors (for instance Koplik & Lasseter 1985; Dias & Payatakes 1986*a* and references therein). If the fluids are Newtonian and if the capillary effects are neglected this approach leads to a linear system of equations in which the unknowns are the fluid pressures at the nodes. At each time step, this system has to be solved and the interface between the fluids updated according to the computed flow rates in the throats (Chen & Wilkinson 1985).

Difficulties arise when capillary effects are taken into account. In this paper, we limit our study to the case of injection of the non-wetting fluid (known as drainage in petroleum literature). In this case, the non-wetting fluid cannot enter a throat as long as the pressure is smaller than a threshold value P_c, given by Laplace's law:

$$P_c = \frac{2\gamma \cos\theta}{r}, \tag{1}$$

where r is the radius of the throat, τ the interfacial tension and θ the contact angle. From a mathematical point of view, the threshold due to the capillary pressure leads to a nonlinear problem: the system of equations used to solve the pressures at each node requires knowledge of which throat will next be invaded by the meniscus, and this knowledge itself requires the value of the pressure at each node.

In order to avoid difficulties due to this nonlinearity, different approaches have been used by the above-mentioned authors. All the methods consist of replacing the nonlinear problem by a sequence of linear problems. Koplik & Lasseter used a 'trial' technique: all possible combinations of elementary displacements are investigated. For each case, the problem becomes linear. Instead of the threshold at the entrance of a cylindrical throat, Dias & Payatakes use the more realistic approximation of a

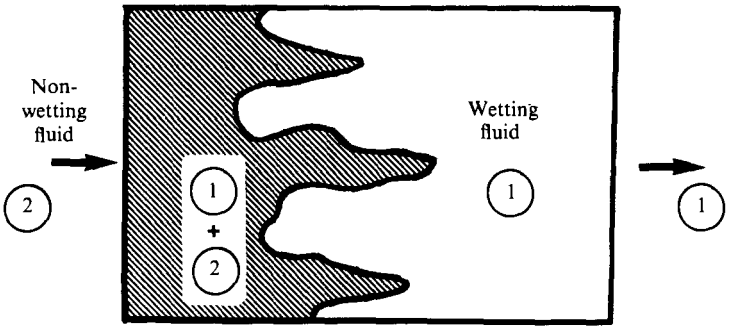

FIGURE 1. Schematic illustration of the linear displacement of the fluid 1 by a fluid 2 in a two-dimensional porous medium.

conical pore. However, the capillary pressure changes during the invasion of the meniscus, and 10–20 steps are necessary to resolve motion in a single throat.

Both methods are time consuming and limited to small networks (10×10 for the first one, 15×30 for the second). Our approach, in this study, is to approximate directly the solution of the nonlinear problem instead of solving a large number of linear problems. This allows us to study networks of dimension 100×100 on a VAX11/785. For the simulation we make the following simplifications which we do not expect to affect the dominant physical mechanisms.

2.2. *Geometry of the network*

The porous medium is represented by means of two sets of elements: pores and throats, situated respectively at the sites and bonds of a regular two-dimensional square lattice. The pores represent the porosity and are spherical. The pressure drops occur only in the throats, which are cylindrial with uniform length. Each element (pore or throat) is thus described by a unique parameter, its radius. These radii are randomly chosen according to a given distribution law (we used here a uniform distribution in an interval $[(1-\sigma)r_0, (1+\sigma)r_0]$ centred on the average radius r_0). A network is thus fully characterized by five parameters: the mean radius and the distribution width for (i) the pores and (ii) the throats, and the distance a between two nodes. In this way, porosity and permeability can be selected independently.

2.3. *Flow conditions*

A first fluid (fluid 1 of viscosity μ_1) in place in the network is displaced by a second one (fluid 2 of viscosity μ_2), injected through a face of the network (figure 1) with no-flow conditions on the lateral boundaries. The pressure is assumed constant at the outlet. Inertial and gravity effects are neglected.

In each pore, we assume a sharp interface between the two fluids (no diffusion or mixing), even when the interfacial tension is very low. This assumption is in good agreement with the observations in micromodels. Consequently, a pore has to be completely filled with the invading fluid before this fluid can reach an adjacent pore. For each pore i, a coefficient α_i gives the percentage of fluid 2 contained in the pore.

We assume that interfacial tension plays a role only when the meniscus is inside the throat: this means that the two adjacent pores are completely filled by different fluids ('interfacial nodes'). Let us examine first the case where there is no capillary effect between pores.

A Poiseuille flow is assumed in each throat. If i and j are two adjacent pores, the flow rate q_{ij} between them is given by

$$q_{ij} = \frac{\pi r_{ij}^4}{8a\mu_{ij}}(p_i - p_j), \tag{2}$$

where r_{ij} is the radius of the throat, p_i and p_j the pressures in pores i and j. The 'effective' viscosity μ_{ij} takes into account the local saturations by means of the average of the two viscosities, weighted with the fraction α of each fluid in the pores:

$$\mu_{ij} = 0.5\,\mu_2(\alpha_i + \alpha_j) + 0.5\,\mu_1(2 - \alpha_i - \alpha_j). \tag{3}$$

This approach is equivalent to introducing a local relative permeability for each fluid, which is a linear function of the saturation.

Now, let us examine the effect of capillarity when the meniscus is in the throat, just between i and j. The flow rate is given by

$$q_{ij} = \frac{\pi r_{ij}^4}{8a\mu_{ij}}(p_i - p_j - P_{ij})^+, \tag{4}$$

where $P_{ij} = 2\gamma \cos\theta / r_{ij}$ is the pressure difference between nodes i and j necessary for the invading fluid (in node i) to enter node j. In this equation, the $+$ denotes the positive part; this means that $q_{ij} = 0$ as long as $(p_i - p_j) < P_{ij}$, otherwise the expression of q_{ij} is the one of a diphasic Poiseuille flow in a tube with a pressure jump at the interface.

The flow between two interfacial nodes no longer depends linearly on the pressure difference: the flow is zero up to a threshold value. The solution of this nonlinear problem is approached through a relaxation technique. At each time step, we sweep the network several times (generally four times), updating the pressure at each node from the pressure of its neighbours through the flow-conservation equation (the flow is taken to be zero between two interfacial nodes as long as the pressure threshold is not reached). We stop when a satisfactory stability is obtained. At this stage, we know the total flow rate and the contents of each pore. The time step is then calculated as the time required to completely fill one pore. This means that the interface is moved in all the pores until it reaches one of the throats.

To illustrate the principle of this nonlinear approach, let us consider the injection through two parallel capillaries, a case that can be studied analytically. The radii of the capillaries are r_1 and r_2 (say $r_1 > r_2$); P_{c_1} and P_{c_2} are the two capillary thresholds ($P_{c_1} < P_{c_2}$); and K_1 and K_2 are the hydraulic conductances ($K = \pi r^4 / 8a\mu$). The invading fluid (non-wetting) is injected at a constant total flow rate q and the fluids have the same viscosities. The pressure P is uniform at the entrance of the tubes and is taken as reference at the exit ($P = 0$).

At time zero, the two menisci are located at the entrances of the two capillary tubes (figure 2*a*). The problem is to determine into which tube the invading fluid will flow and calculate the pressure P at the entrance and the flow rate in each tube as a function of the total flow rate q.

Figure 2(*b*) shows an example with the numerical values $P_{c_1} = 1.68$; $P_{c_2} = 2$; $K_1 = 2$; $K_2 = 1$. The solid line represents the nonlinear relation between q and P (analogous to (4)):

$$q = K_1(P - P_{c_1})^+ + K_2(P - P_{c_2})^+. \tag{5}$$

This equation contains all the physics of the displacement:

As long as P is smaller than P_{c_1}, each of the two terms of q (5) is nil and there is no displacement.

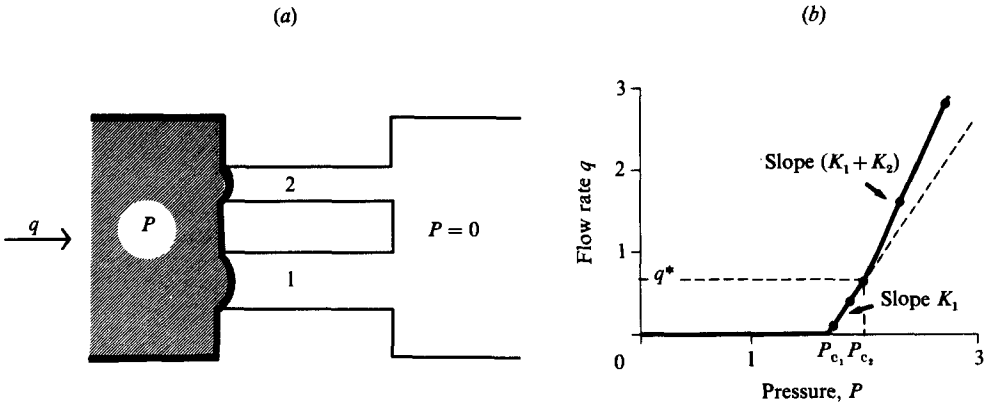

FIGURE 2. Injection of a non-wetting fluid into two parallel capillaries: (*a*) situation at time zero, (*b*) nonlinear relationship between the flow rate q and the pressure P.

When P is between P_{c_1} and P_{c_2}, only the first term is not nil, and the fluid flows into the first tube (the largest) with a conductance K_1 (slope of the segment).

If $P > P_{c_2}$, the fluid flows in both tubes, with a total conductance $K_1 + K_2$ (slope of the segment).

In our problem we impose the flow rate, and the unknown pressure is calculated directly by means of this *nonlinear* relationship between q and P. We can see that below q^* (corresponding to P_{c_2}), the injected fluid only enters tube 1, while above it enters both tubes.

In the simulator the nonlinear equation is solved by using a relaxation process. The dots on figure 2(*b*) are the numerical results for the pressures corresponding to different flow rates obtained using this technique.

The method of Koplik & Lasseter (1985) in this simple case, would consist in first making the hypothesis that the fluid flows only into tube 1, computing the corresponding pressure, checking if $P < P_{c_2}$ and, if not, recomputing the pressure assuming that the fluid flows into both tubes. Dias & Payatakes (1986*a*) would replace the cylindrical tubes by conical throats and compute step by step the menisci displacements.

2.4. *Results of the simulations*

We are dealing with three kind of forces: viscous forces in fluid 1, viscous forces in fluid 2, and capillary forces. Consequently, an experiment or a simulation is fully characterized by two dimensionless numbers, which are the ratios of two different forces. We arbitrarily choose the viscosity ratio $M = \mu_2/\mu_1$, and the capillary number C, which is the ratio between viscous forces which act at the pore scale in the injected fluid and capillary forces:

$$C = \frac{q\mu_2}{\Sigma\gamma\cos\theta}, \tag{6}$$

where Σ is the cross-sectional area of the sample. For both simulations and experiments, Σ is the product of the width of the network by a thickness equal to the distance between two sites (1 mm).

With this assumption, each simulated displacement can be displayed as a point in a plane with axes representing the vicosity ratio and the capillary number. Owing to the large variation of these parameters, the two axes are presented in decimal logarithmic scales.

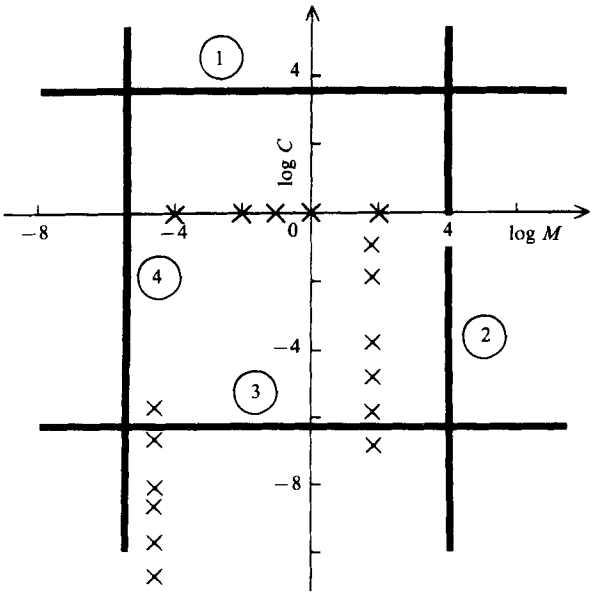

FIGURE 3. Locations of the various simulations in the plane M–C on a log–log scale: × represents the 100×100 simulations and the four lines 1 to 4 the 25×25 ones.

We used two different networks: a large one (100×100), computer-time consuming but with a size close to the experimental micromodels, and a small one (25×25), which allows a detailed exploration of the plane M–C.

100×100 *network*

The parameters describing the geometry of the pores are chosen to represent the experimental values of the micromodel (see §4.1). The mean radius of the pores is equal to the mean radius of the throats (micromodels are made of interconnected capillaries) $r_0 = 0.23$ mm, with a dispersion $\sigma = 0.5$ for the throats and 0.2 for the pores. We have checked that monophasic permeability is in good agreement with the experimental one. The geometrical network is the same for all the simulations.

The results consist of two series of simulations at different C and constant M and a series at constant C. The corresponding points are represented by crosses, located on the M–C diagram shown in figure 3. The simulations are run until the injected fluid (2) reaches the opposite face, when 'breakthrough' is said to have occurred. In figure 4 (a–c) we show in black the pores occupied by the invading fluid at the moment of breakthrough.

The first series of simulations (figure 4a) shows the evolution of the pattern with the capillary number when a less-viscous fluid is injected ($\log M = -4.7$; $M = 2 \times 10^{-5}$). At high flow rate, the pattern remains the same for the two highest value of C. This pattern is characteristic of *viscous fingering*. At very low C, we find a different pattern caused by *capillary fingering* ($\log C = -9.7$ and -10.7).

In the second series (figure 4b), a more-viscous fluid is injected; the viscosity ratio is $M = 79$ ($\log M = 1.9$). We observe a continuous transition between two different well-defined patterns; the first one at very low flow rate ($\log C = -5.9$ and -6.9) when capillary effects are dominant and the second one at high flow rate ($\log C = -0.9$ and -1.9), corresponding to a *stable displacement* (displacement stabilized

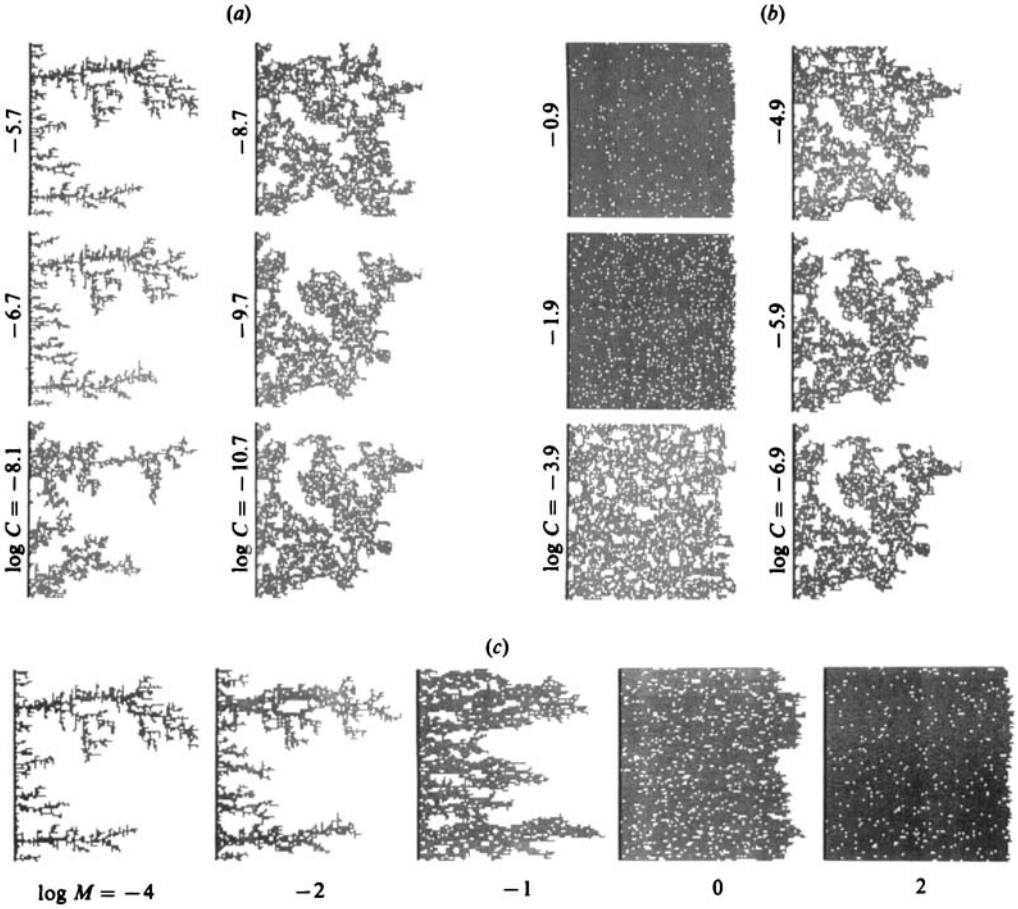

FIGURE 4. 100 × 100 simulations at various viscosity ratio and capillary numbers: (*a*) $\log M = -4.7$, from viscous fingering to capillary fingering; (*b*) $\log M = 1.9$, from stable displacement to capillary fingering; (*c*) $\log C = 0$, from viscous fingering to stable displacement.

by viscous effects). At low flow rate, the pattern due to capillary effects is identical with the one obtained in the unstable case (figure 4*a*, $\log C = -10.7$).

The third series at constant capillary number ($\log C = 0$) shows the transition between the two patterns which characterize *viscous fingering* and *stable displacement* (figure 4*c*). The two extreme patterns are also identical with the corresponding ones from the two previous simulations (figure 4*a*,*b* at the highest C).

We may quantify the evolution of the patterns by means of the pore volume fraction S of the injected fluid at breakthrough (equivalent to the partial saturation in fluid 2) and the results are shown in figure 5. The dots correspond to the same geometrical distribution of pores and throats (same seed for the random generator). For $\log M = 1.9$, the saturation S increases monotonically from 0.37 at low C (capillary fingering) to 0.95 for the stable displacement. In the other series at constant viscosity ratio ($\log M = -4.7$) the saturation presents a maximum ($S = 0.40$) and a minimum ($S = 0.15$), between two plateaux ($S = 0.37$, capillary fingering and $S = 0.22$ viscous fingering). The third curve at $\log C = 0$ increases monotonically from $S = 0.22$ (viscous fingering) to 0.95 (stable displacement).

The results obtained with a different seed for the random generator are plotted in

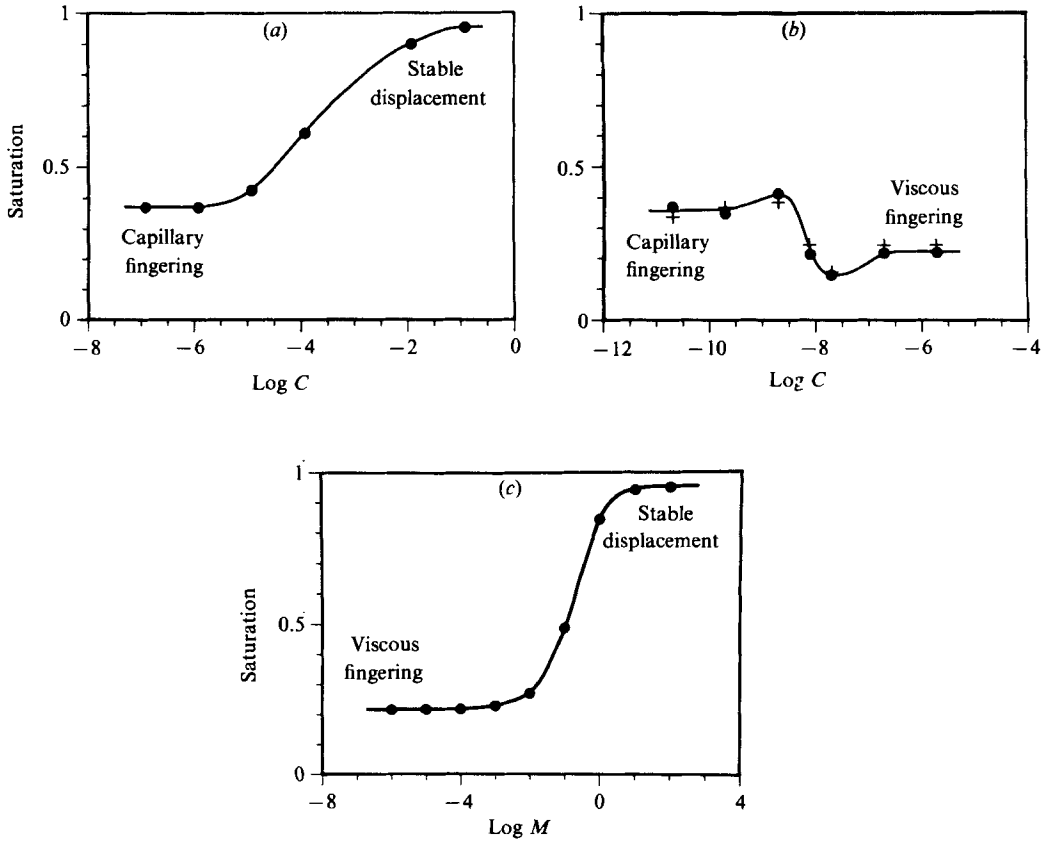

FIGURE 5. 100×100 simulations: plot of the fraction of invading fluid at breakthrough: (*a*) $\log M = 1.9$; (*b*) $\log M = -4.7$; (*c*) $\log C = 0$. The black dots and the crosses represent the results of the simulations.

figure 5(*b*) (crosses). The fluctuations are small, a result expected when using a large network.

An interesting question is the evolution of the patterns and of the final saturations over a large range of viscosity ratios M. For this purpose we must use a smaller network in order to limit the CPU time.

25×25 network

The mean radius of the pores and throats is $r_0 = 0.56$ mm; the dispersion $\sigma = 0.7$ for the throats and 0.2 for the pores. All the simulations were performed with the same network. We first explored the four lines shown in figure 3. All the saturation curves (figure 6) have the same shape: two plateaux for the extreme values for M or C and a transition zone. The results are similar to the 100×100 simulations but, owing to the difference of size of the networks and pores size distribution, the height and position of the plateaux are somewhat different. Subsequent exploration of the entire plane leads to three domains, corresponding to the plateaux of the previous curves, within which the saturation S is constant: $S = 0.28$, 0.54 or 0.80. The boundaries of these domains are displayed in figure 7.

Inside a constant-saturation domain, the simulated patterns remain identical (for a given network). Outside the domains, the patterns evolves continuously toward a

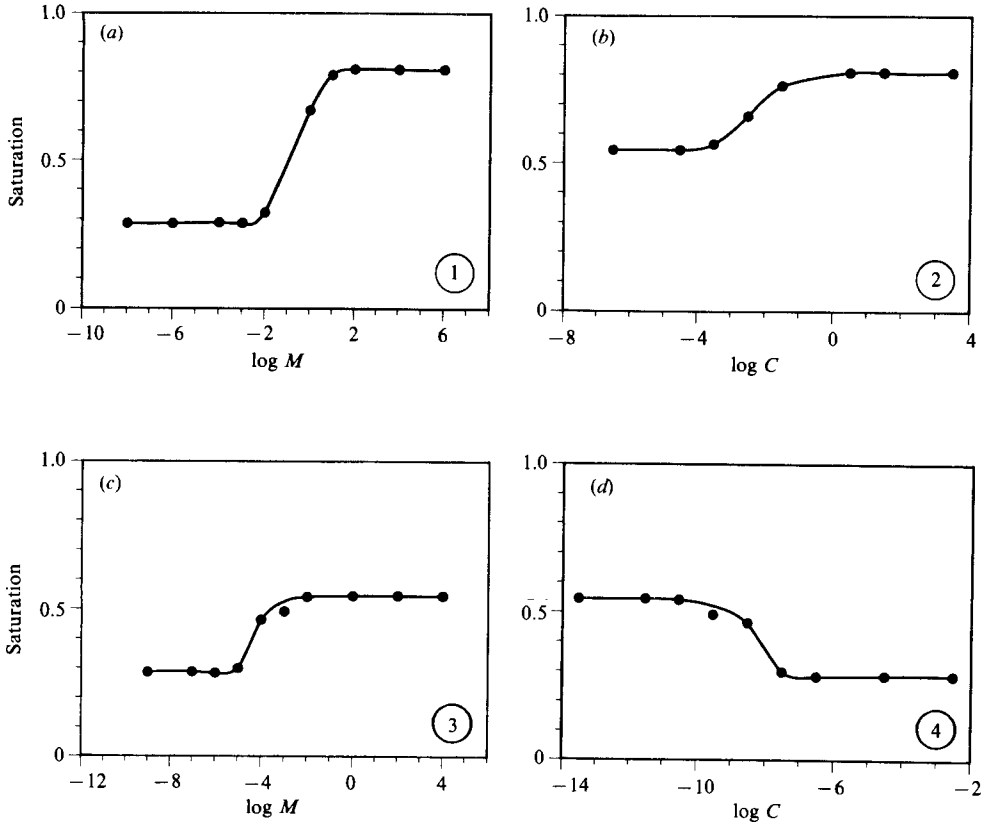

FIGURE 6. Plot of the fraction of invading fluid at breakthrough in the 25×25 simulations along the lines 1–4 shown in figure 3. (*a*) $\log C = 3.5$; (*b*) $\log M = 4$; (*c*) $\log C = -6.5$; (*d*) $\log M = -6$.

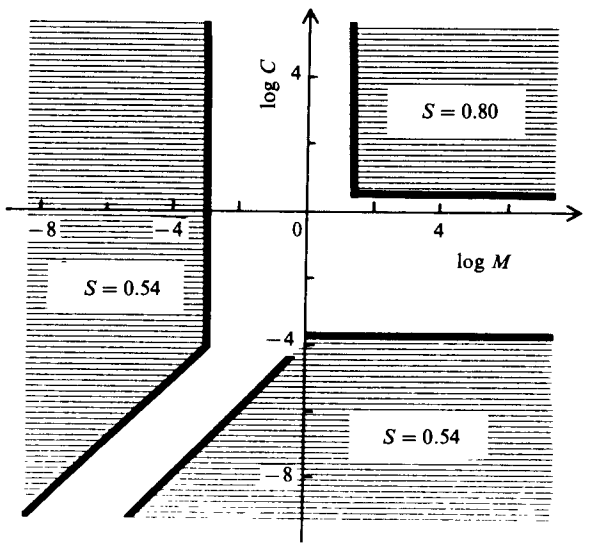

FIGURE 7. Plot of the constant-saturation domains for the 25×25 simulations.

new pattern characteristic of another domain, in the same way as the two series obtained with the 100×100 network.

The mapping of these three domains in the plane M–C, for a given geometry and size of the network constitutes the 'phase-diagram' for this given network.

3. The phase-diagram

How can we physically justify these domains and the shapes of their boundaries?

3.1. *Physical interpretation of the domains*

Each of these three domains corresponds to a different 'basic' mechanism where only one kind of force is acting, the two others being negligible at the scale of the network studied:

(i) *Stable displacement*: the principal force is due to the viscosity of the injected fluid; capillary effects and pressure drop in the displaced fluid are negligible. The pattern presents a flat front with some irregularities at the scale of a few pores (figure 4*b*, $\log C = -0.9$). The size of the clusters trapped behind the front is also only a few pores.

(ii) *Viscous fingering*: the principal force is due to the viscosity of the displaced fluid; capillary effects and pressure drop in the displacing fluid are negligible. The tree-like fingers present no loops, they spread across the whole network and they grow towards the exit (figure 4*a*, $\log C = -5.7$).

(iii) *Capillary fingering*: at low capillary number the viscous forces are negligible in both fluids and the principal force is due to capillarity. The fingers also spread across the network but the pattern is different from the previous case and the final saturation is larger (figure 4*a*, $\log C = -10.7$ and figure 4*b*, $\log C = -6.9$). At all scales, the fingers grow in all directions, even backward (toward the entrance). They form loops which trap the displaced fluid and the size of the trapped clusters ranges from the pore size to macroscopic, of the order of the network size.

3.2. *Boundaries of the domains*

Comparison between different simulations shows that changing the pore size distribution or the size of the network leads to a translation of the boundaries of the domains but that the general shape remains unchanged. We can *qualitatively* justify this result, which is the main property of the phase-diagram.

Based on the value of the viscosity ratio M, one can distinguish three zones (figure 8): zone I, at very low M, where viscous forces in the injected fluid (2) are negligible in comparison with viscous forces in the displaced fluid (1); zone II, the transition zone, where the viscous pressure drops in both fluids play a significant role; and zone III, at very large M, where the viscous pressure drop in fluid 1 is negligible. The viscous pressure drop δP across the network in each fluid can be calculated by using the relative permeability k_r (generalized Darcy's law):

$$\delta P = \frac{\mu q L}{k k_r \Sigma}, \tag{7}$$

where Σ is the cross-sectional area of the sample and k the monophasic permeability. The calculation of k_r is beyond the scope of this paper; however, its value remains constant inside each of the domains.

Now, varying the capillary number of changes the relative importance of capillary effects compared with viscous forces:

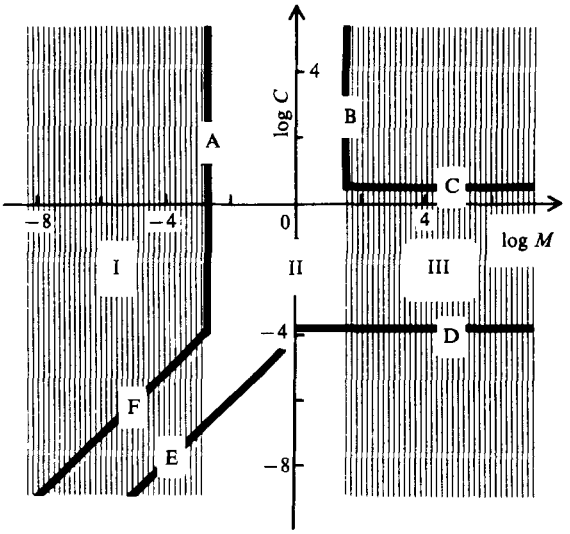

FIGURE 8. Schematic representation of the three zones where the different viscous forces are acting and the boundaries of the basic domains (lines A–F).

At high C: the capillary forces are negligible. In this case, zone I corresponds to the domain where viscous forces in fluid 1 are dominant (viscous fingering) and zone III to the domain of stable displacement. The boundaries of these two domains, at high C, are the limits of zones I and III, i.e. the lines A and B parallel to the C-axis (figure 8).

At low C: viscous forces, which act on the length L of the network, are very small in comparison with capillary forces, i.e

$$\frac{\mu q L}{k k_r \Sigma} \ll \frac{\gamma \cos\theta}{r}. \tag{8}$$

In zone III, viscous forces are dominant in fluid 2 and $\mu = \mu_2$. Consequently, this leads to the equation of the boundary of the capillary domain:

$$\mu_2 q L = \text{constant} \times \frac{\gamma \cos\theta}{r}, \tag{9}$$

which leads to $C = \text{constant} \times k k_r / rL$, a condition represented by a line parallel to the M-axis (line D, figure 8).

In zone I, viscous forces are dominant in fluid 1 with $\mu = \mu_1$ in (8). This leads to an equation of the form $C = \text{constant} \times M \times k\, k_r / r$, which gives a line with a slope = 1 in log–log scale (line E, figure 8).

In zone II, we can only assume continuity between lines E and D.

At intermediate C: the effect of capillary forces becomes negligible when

$$\frac{\gamma \cos\theta}{r} \ll \frac{\mu q L}{k k_r \Sigma}. \tag{10}$$

The calculation is analogous to the previous case (with a different constant) and gives two lines which are parallel to the boundaries of the capillary domain (lines C and F, figure 8).

Note that the slope = 1 (in zone I) is due to the definition of the capillary number

by reference to fluid 2. In fact the significant pressure drop is in the more-viscous fluid and we should use a capillary number based on the larger viscosity in order to represent the real mechanisms. However, we must keep the same definition of C to draw the diagram.

So far we have presented the results based on computer simulations. We now check the validity of this approach by experiments performed in two-dimensional artificial porous media.

4. Experimental set-up

Experiments in micromodels are a complement to computer simulations at two levels: first, they provide information on the physical mechanisms that take place at the pore level and, secondly, they test the validity of the model by comparing the results on a large scale. For the detailed study of the mechanisms at the pore level during drainage, and a description of the micromodel, we refer the reader to Lenormand, Zarcone & Sarr (1983). The purpose of the following section is to compare the large-scale patterns obtained with the simulations.

4.1. *Micromodels*

We have developed a moulding technique using a transparent resin and a photographically etched mould. The cross-section of each duct is rectangular with a constant depth ($e = 1$ mm) and a width d which varies at random from pore to pore. For this study we used a large network (135×150 mm) containing about 42 000 ducts with seven classes of width (from 0.1 to 0.6 mm), distributed with a log–normal law. The distance between two sites of the network is 1 mm and the permeability k is approximately 10^{-9} m^2 (1000 Darcy).

For the whole set of experiments we used four micromodels, all made from the same mould.

4.2. *Fluids*

Various fluids have been used in order to vary the capillary number and the viscosity ratio over a large range:

Aliphatic oils, used as wetting fluids, coloured with a red organic dye (except when mercury is used as a non-wetting fluid). The viscosity ranges from 0.32 cP (or 0.32×10^{-3} Pa s) to 1000 cP.

Glucose aqueous solution, with viscosity from 1 cP (pure water) to 1000 cP, used as non-wetting fluid with oil. Owing to the nature of the resin of the micromodel, this pair of fluids is only suitable for experiments of short duration (less than one hour). For long experiments, the contact angle varies and the wettability is not well defined.

Air (viscosity 180 μP), used as non-wetting fluid with oil or as wetting fluid with mercury.

Mercury, always a non-wetting fluid (viscosity 1.55 cP). This fluid presents no evolution of the contact angle with time. It can therefore be used for very long experiments. Furthermore, its high surface tension and low viscosity lead to very low capillary numbers.

The non-wetting fluid is injected through the micromodel (drainage) using constant-flow-rate syringe pumps (volumetric flow rate q) at room temperature.

Run	μ_2 cP	μ_1 cP	γ dyn/cm	q cm^3/s	R_1	R_2	log M	log C
A–O 1	0.018	1000	20	8.3×10^{-2}	6×10^{-4}	4×10^{-2}	−4.7	−6.3
A–O 2	0.018	1000	20	2.8×10^{-2}	2×10^{-4}	1×10^{-2}	−4.7	−6.7
A–O 3	0.018	1000	20	1.3×10^{-3}	1×10^{-5}	6×10^{-4}	−4.7	−8.1
A–O 4	0.018	1000	20	1.1×10^{-4}	8×10^{-7}	5×10^{-5}	−4.7	−9.1
Hg–O 1	1.55	1000	370	2.8×10^{-2}	2×10^{-4}	2	−2.8	−6.1
Hg–O 2	1.55	1000	370	5.6×10^{-3}	4×10^{-5}	0.4	−2.8	−6.8
Hg–O 3	1.55	1000	370	8.3×10^{-4}	6×10^{-6}	5×10^{-2}	−2.8	−7.6
Hg–O 4	1.55	1000	370	8.3×10^{-5}	6×10^{-7}	5×10^{-3}	−2.8	−8.6
Hg–O 5	1.55	1000	370	1.4×10^{-5}	1×10^{-7}	9×10^{-4}	−2.8	−9.4
Hg–O 6	1.55	100	410	2.8×10^{-2}	2×10^{-3}	2	−1.8	−6.1
Hg–O 7	1.55	100	410	5.6×10^{-3}	4×10^{-4}	0.4	−1.8	−6.8
Hg–O 8	1.55	100	410	8.3×10^{-4}	6×10^{-5}	5×10^{-2}	−1.8	−7.6
Hg–O 9	1.55	100	410	8.3×10^{-5}	6×10^{-6}	5×10^{-3}	−1.8	−8.6
Hg–O 10	1.55	100	410	1.4×10^{-5}	1×10^{-6}	9×10^{-4}	−1.8	−9.4
Hg–O 11	1.55	5.6	450	2.8×10^{-2}	4×10^{-2}	2	−0.6	−6.1
Hg–O 12	1.55	5.6	450	5.6×10^{-3}	8×10^{-3}	0.4	−0.6	−6.8
Hg–O 13	1.55	5.6	450	9.4×10^{-4}	1×10^{-3}	5×10^{-2}	−0.6	−7.6
Hg–O 14	1.55	5.6	450	8.3×10^{-5}	1×10^{-4}	5×10^{-3}	−0.6	−8.7
Hg–O 15	1.55	5.6	450	1.4×10^{-5}	2×10^{-5}	9×10^{-4}	−0.6	−9.4
Hg–H 1	1.55	0.32	470	3.8×10^{-1}	9	20	0.7	−5.0
Hg–H 2	1.55	0.32	470	2.8×10^{-2}	0.7	2	0.7	−6.2
Hg–H 3	1.55	0.32	470	8.3×10^{-4}	2×10^{-2}	5×10^{-2}	0.7	−7.7
Hg–H 4	1.55	0.32	470	8.3×10^{-5}	2×10^{-3}	5×10^{-3}	0.7	−8.7
Hg–A 1	1.55	0.018	480	1.6	0.8	100	1.9	−4.4
Hg–A 2	1.55	0.018	480	3.2×10^{-1}	0.2	20	1.9	−5.1
Hg–A 3	1.55	0.018	480	4.7×10^{-2}	2×10^{-2}	3	1.9	−5.9
Hg–A 4	1.55	0.018	480	3.2×10^{-4}	2×10^{-4}	2×10^{-2}	1.9	−8.1
W–O 1	570	5.6	14.5	3.2×10^{-1}	4×10^{-1}	4×10^{-3}	2	−1.0
W–O 2	570	5.6	14.5	3.2×10^{-3}	4×10^{-3}	4×10^{-5}	2	−3.0
W–O 3	570	5.6	14.5	6.0×10^{-4}	8×10^{-4}	8×10^{-6}	2	−3.8
W–O 4	570	5.6	14.5	2.2×10^{-5}	3×10^{-5}	3×10^{-7}	2	−5.2
W–O 5	4700	5.6	14.5	5.8×10^{-2}	8×10^{-2}	9×10^{-5}	2.9	−0.9
W–O 6	4700	5.6	14.5	3.3×10^{-3}	4×10^{-3}	5×10^{-6}	2.9	−2.1
W–O 7	4700	5.6	14.5	1.1×10^{-3}	2×10^{-3}	2×10^{-6}	2.9	−2.6
W–O 8	4700	5.6	14.5	1.8×10^{-4}	2×10^{-4}	3×10^{-7}	2.9	−3.4

TABLE 1. Physical properties of the fluids and flow conditions

4.3. *Characterization of the experiments*

In the same way as for the network simulator, the two main parameters are the viscosity ratio and the capillary number, with the same definitions. The capillary pressure is calculated in a channel with a rectangular cross-section ($d\times e$) by the equation

$$P_c = 2\gamma\cos\theta\left(\frac{1}{d}+\frac{1}{e}\right), \tag{11}$$

with less than 6% error (Lenormand *et al.* 1983).

However, we cannot completely avoid gravitational and inertial effects:

gravitational forces; the micromodel is held horizontal in order to avoid gravity effects. Some problems might occur with mercury when the horizontality is not

perfect (the pressure due to height of 1 mm of mercury is 130 Pa, compared to the capillary pressure of 1000 Pa in a 1 mm diameter channel).

inertial forces; the Reynolds number R (ratio between inertial and viscous forces) is calculated within a channel by the classical definition

$$R = \frac{\rho V d}{\mu}. \tag{12}$$

In this equation, the calculation of the velocity V depends upon the flow pattern: for a piston-like displacement, the fluids are moving in all channels across the section of the micromodel (assumed to be equivalent to a bundle of N parallel channels). For a finger-like displacement, we assume flow through only one channel. The two values of Reynolds number (fluids 1 and 2) are always very small (creeping flow, $R \ll 1$), except for mercury because of its high density.

All the parameters describing the various experiments are collected in table 1.

The measurement of the final saturation at breakthrough is not accurate or sufficiently reproducible to be a useful parameter, the main problems being the differences in behaviour of two pairs of fluids (due to the contact angle and trapping mechanisms at the pore level) and small differences in the etching of the micromodels (see below the discussion section).

5. Experimental results

We present only the most significant experiments, which are indicated on figure 9, and referenced by the initials of the fluids, the first one corresponding to the non-wetting fluid. The non-wetting fluid is always injected at the left-hand side of the micromodel, but, depending on the nature of the fluids, it may appear as white or black in the pictures.

Air/oil (A–O): $\log M = -4.7$ (figure 10*a*).

Mercury/hexane (Hg–H): $\log M = 0.7$ (figure 10*b*).

Mercury/air (Hg–A): $\log M = 1.9$ (figure 10*c*).

Water–glucose/oil (W–O): $\log M = 2$ (figure 10*d*) and $\log M = 2.9$ (figure 10*e*).

Mercury/oil (Hg–O): $\log M = -2.8$, -1.8 and -0.6 (figure 11).

The whole set of experimental results agrees with the results of the computer simulations: we can identify the three domains corresponding to stable displacement, viscous fingering and capillary fingering. Inside each domain the general shapes of the experimental patterns are similar to the simulations. Between these domains we also observe the transition zones within which the patterns vary continuously from one structure to another.

5.1. *Basic mechanisms*

Unlike the simulations we have no parameter S to decide when the plateau is reached and, consequently, our selection of the experiments that correspond to basic mechanisms is based solely on the aspect of the patterns within each series of experiments.

Stable displacement: The frontier between the fluids is flat and the amount of fluid trapped behind the front is very small. Experiment W–O 5 (figure 10*e*) corresponds to this case (see injection conditions in table 1).

Capillary fingering: This kind of displacement is illustrated by experiments Hg–A 4 (figure 10*c*, mercury displacing air with $C \approx 10^{-8}$) or Hg–O 8, 9, 10, 12 (figure 11).

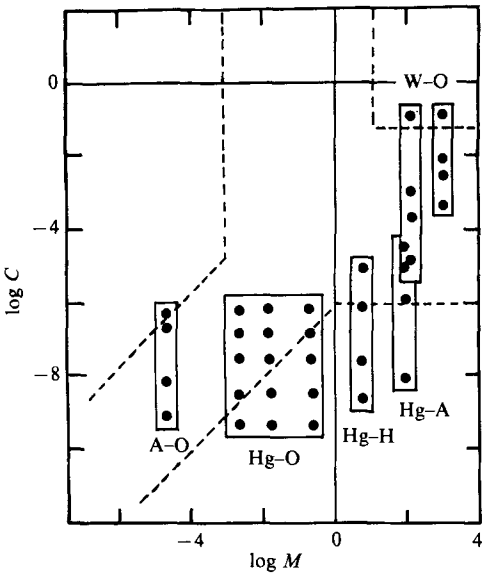

FIGURE 9. Locations of the various series of experiments in the plane M–C. The letters represent the various fluids: A: air, Hg: mercury, O: oil, H: hexane and W: glucose–water solution. The dashed lines are the limits of the basic domains, from the 100×100 simulations.

Viscous fingering: Figure 12 shows four stages of the injection of air (white) through very viscous oil (black). The conditions of injection are approximately the same as for experiment A–O 1 (table 1). Initially, several small fingers grow at the entrance of the micromodel and, progressively, a few of them grow faster than their neighbours and inhibit the development of the shorter fingers. The aspect of the fingers is different from the capillary case: no loops can be seen and all the fingers are oriented toward the exit; this leads to a characteristic tree-like shape.

5.2. *Cross-over: stable displacement–capillary fingering*

Owing to technical limitations, (pressure, time, etc.) we cannot use the same pair of fluids for studying the whole transition zone: we used water/oil for high C and mercury with air or hexane for low C. The behaviour of the different series is quite coherent:

Stable displacement when $\log C > -1$ (W–O 1 and 5).

Capillary fingering when $\log C < -7$ (Hg–H 3 and 4 and Hg–A 4). However, the patterns differ between air and hexane; this may be due to a small difference of etching in the micromodels. Another possibility is linked to the low viscosity of air: when trapped by mercury, air can easily escape by flowing along the roughness of the walls (the 'leak' mechanism, Lenormand & Zarcone 1984*a*).

Transition zone. Decreasing the flow rate (or C) increases progressively the extension of fingering from pore size (stable displacement) to the size of the network. The amount of trapped phase also increases with the length of the fingers. Furthermore, the size of the trapped blobs is of the order of the finger size.

5.3. *Cross over: capillary fingering–viscous fingering*

Figure 11 displays the results at breakthrough for three viscosity ratios and five capillary numbers with the fluids mercury oil. All the experiments of this series are performed with the same micromodel. We observe a constant pattern corresponding

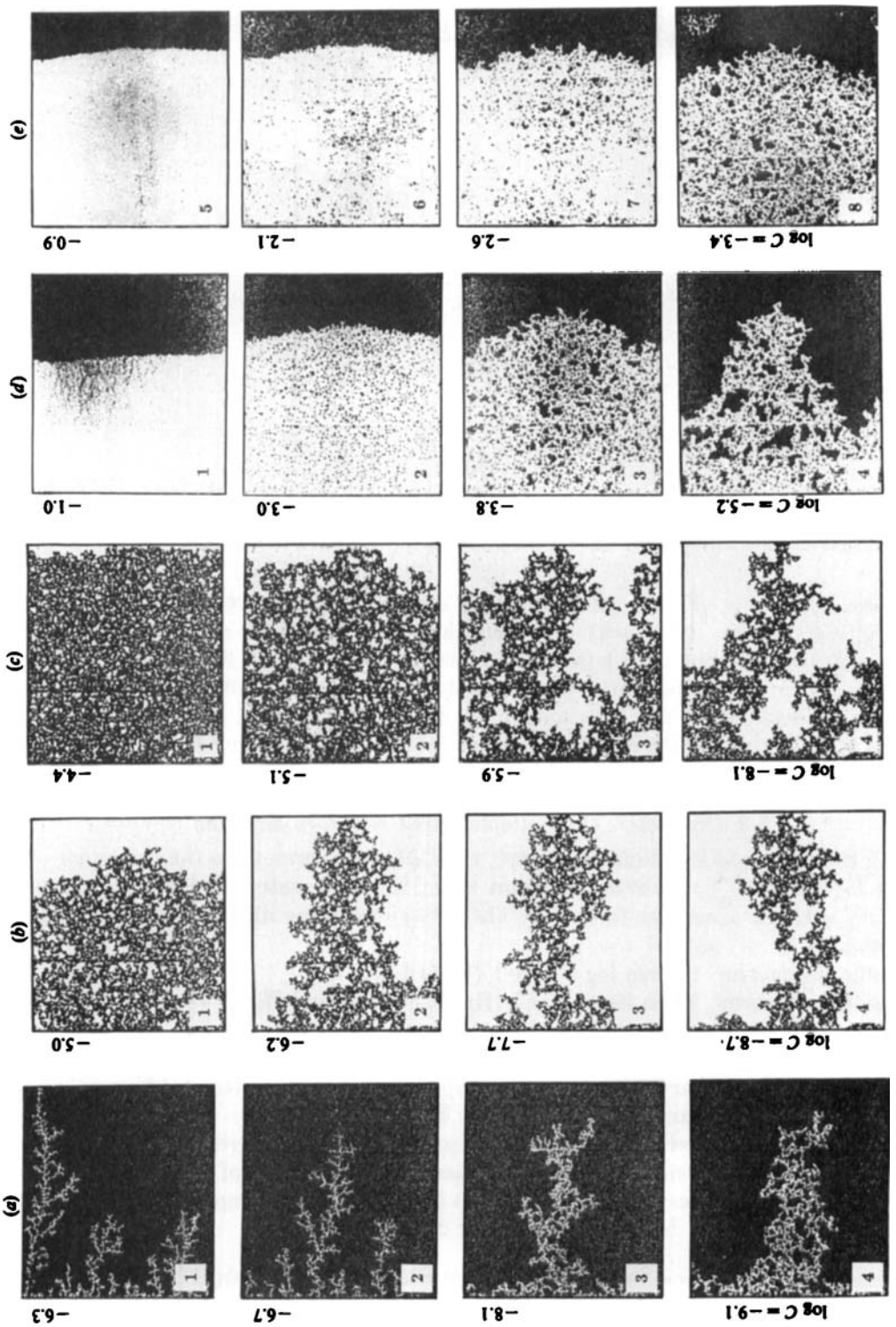

FIGURE 10. (*a*) Air (white) displacing a very viscous oil at various C at $\log M = -4.7$: from viscous fingering (1) to capillary fingering (4). (*b*) Mercury (black) displacing hexane at $\log M = 0.7$. (*c*) Mercury (black) displacing air at $\log M = 1.9$. (*d*) Glucose solution (white) displacing oil at $\log M = 2.0$ and various C: from stable displacement towards capillary fingering. (*e*) Glucose solution (white) displacing oil at $\log M = 2.9$ and various C: from stable displacement towards capillary fingering.

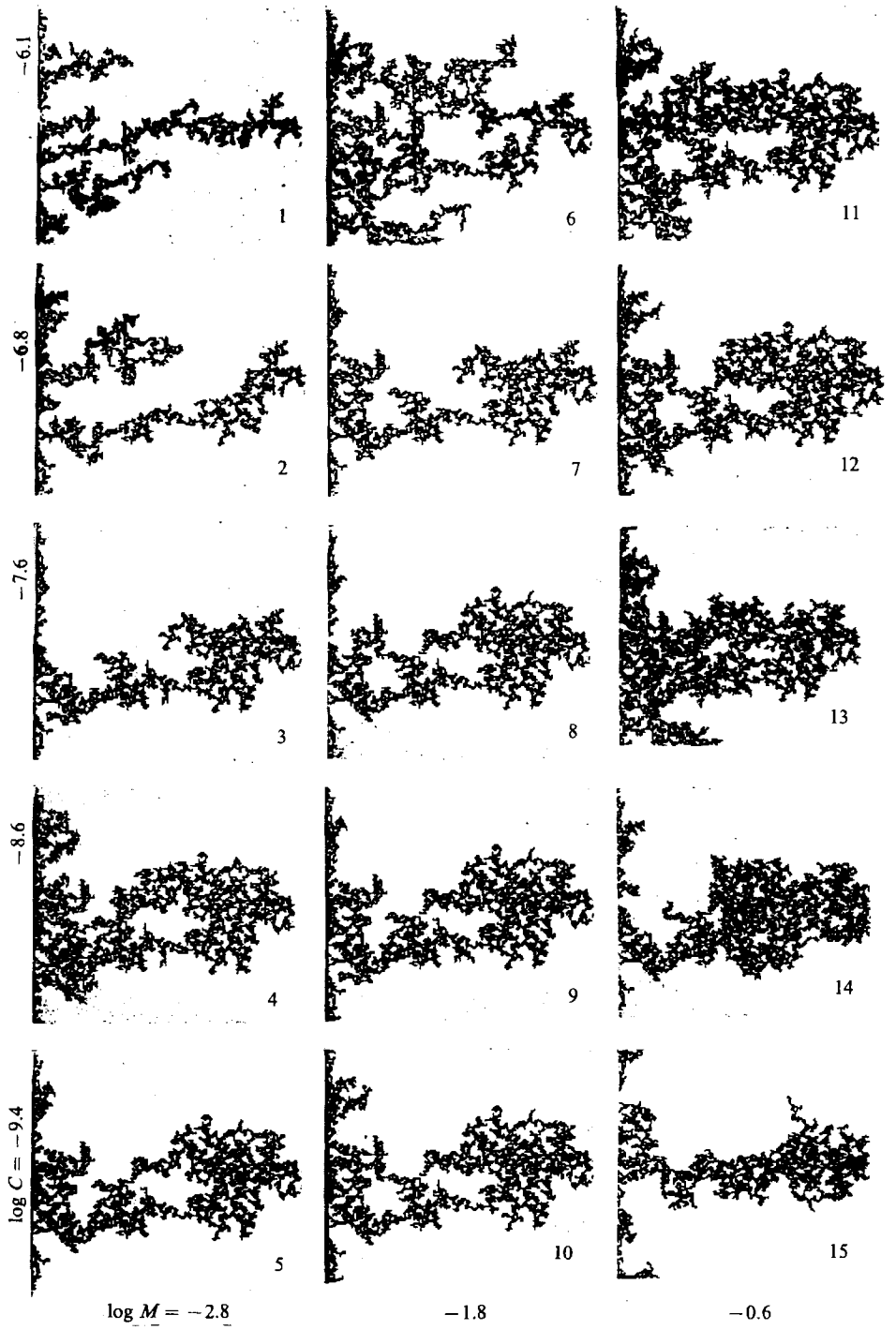

FIGURE 11. Mercury (black) displacing three various types of oils at different C and M. All the experiments are performed in the same micromodel.

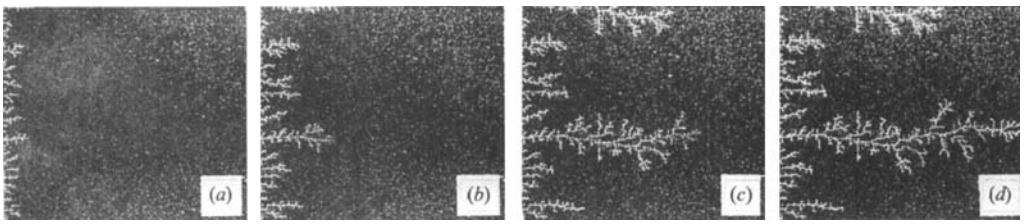

FIGURE 12. Different stages of the displacement of a very viscous oil by air.

to capillary fingering (pictures 4, 5, 8–10 and 12–15). The analogy between the patterns proves that capillary fingering is deterministic. The left-hand column ($\log M = -2.8$) shows the effect of viscous forces when the flow rate increases: fingers become progressively thinner and the number of backward branches decreases (pictures 3 to 1). However picture 1 remains different from tree-like viscous fingers.

In figure 10*a*, the choice of viscous oil (1000 cP) and air leads to a very low viscosity ratio, a necessary condition for a strong viscous instability. The four pictures show the transition between viscous fingering (A–O 1 and 2) towards capillary fingering.

5.4. *Comparison with simulations*

First, we want to underline the experimental difficulties which may affect the results:

Damaged micromodels: the fluids used for cleaning can cause large changes of wettability or permeability. For instance, the micromodel used in the experiments Hg–O or A–O seems more permeable in the centre zone than along the edges, a default that is more sensitive to capillary effects than viscous effects (A–O 4, for instance).

Wettability problems, with oil and water at very low flow rate.

Gravity, with mercury.

Some problems are due to the physical properties of the fluids and cannot be overcome without changing the experimental technique. The most important is the effect of inertial forces present in mercury. For instance, the Reynolds number in mercury is very high for Hg–A 1 and 2 (table 1) and these two experiments should be presented more as a cross-over towards inertial effects rather than viscous effects. However, near the percolation frontier (Hg–A 4), this effect is negligible ($R = 5 \times 10^{-3}$).

The second problem is the displacement of the trapped blobs at very high capillary number. This effect is not an artifact due to the micromodel, and does indeed take place during enhanced oil recovery in real rock samples. However our simulator cannot account for this mechanism, unlike that developed by Dias & Payatakes (1986*b*).

Despite these technical problems, the comparison between experimental and numerical result leads to a good agreement for:

The existence of the three basic mechanisms and the similarity of the experimental and simulated patterns in each domain: capillary fingering, viscous fingering or stable displacement.

The extension of cross-over zones: a large gap (around 4 decades) between stable displacement and capillary fingering and a smaller gap (3 decades) between capillary fingering and viscous fingering.

Good agreement for the location of the boundaries of the phase-diagram. To allow comparison, we have plotted as dashed lines (figure 9) the boundaries obtained from the three series of simulations, assuming the same shape as for the 25×25 simulations (figure 7). From the previous determination of the experimental basic domains, we can conclude that we have an agreement within the order of the decade. For example, the simulated boundary for the capillary domain crosses the matrix of experiments Hg–O (figure 11) through the pictures 4, 8, 12, which fits with the visual determination.

Consequently, the relatively good agreement between the experiments and the simulations validates the microscopic rules used in the network simulator. Note that experiments in the reverse case of imbibition (wetting fluid displacing non-wetting fluid) lead to different results, indicating that the same microscopic laws based on the analogy with flow through smooth capillary tubes cannot be utilized for imbibition (flow along the roughness of the walls, snap-off mechanisms, etc., Lenormand & Zarcone 1984*a*).

The second conclusion is that both the experiments in micromodels and the network simulator justify the notion of a phase-diagram.

We shall now show how these patterns can be described by a stochastic approach.

6. Statistical modelling of the basic mechanisms

In this section, our purpose is to associate a well-defined statistical model with each of the three different patterns of the basic mechanisms (stable displacement, viscous fingering and capillary fingering).

A continuum approach based on the macroscopic Darcy's law cannot describe the ramified and chaotic aspect of both capillary and viscous fingers. Consequently, alternative models based on a microscopic description of the medium and stochastic displacement of the interface between the fluids have been developed. Such stochastic models lack the physical description of the network simulators, but are still capable of useful predictions of the geometry and transport properties of a given network, and of how these properties depend on the network size. Furthermore, statistical simulations on a computer are generally faster than solving flow equations in network simulators.

Our purpose is not to describe these theories in detail, but rather to recall the main feature already obtained in previous studies and give the more recent references.

6.1. *Capillary fingering and invasion percolation*

This approach is related to capillary mechansims that take place at the microscopic (pore) scale and the randomness due to the different sizes of pores.

Capillary forces prevent the non-wetting fluid from spontaneously entering a porous medium. It can only enter a throat (radius r^*) when the pressure exceeds the pressure in the wetting fluid by a value P_c equal to the 'capillary pressure'. From a statistical point of view a duct with $r > r^*$ is an 'active' or 'conductive' bond and a duct with $r < r^*$ an inactive bond.

At a given pressure P_c, the injected fluid invades all the channels connected to the injection face; this mechanism is called 'invasion percolation' (see for instance Wilkinson 1985 and references therein). During the displacement, the wetting phase is trapped in the network when the invading non-wetting fluid breaks the continuous path toward the exit.

A computer simulation of invasion percolation is based on the following rules. A

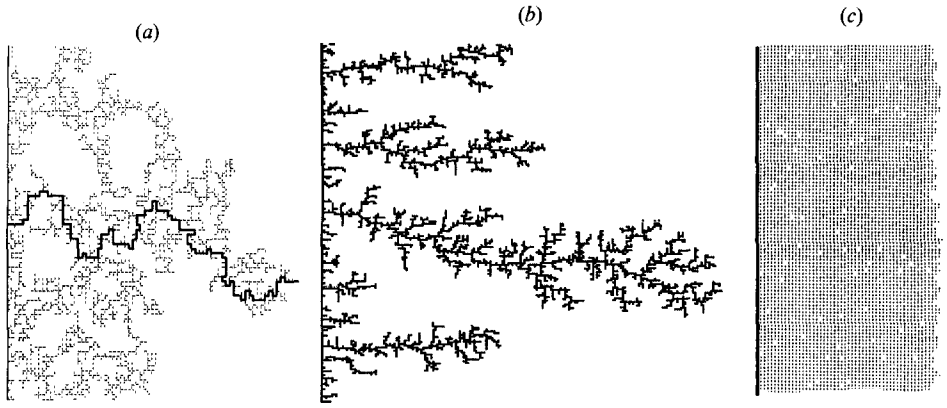

FIGURE 13. Results of statistical simulations on a large network: (*a*) invasion percolation, (*b*) diffusion-limited aggregation with a line seed, (*c*) anti-DLA.

random number (a probability between 0 and 1) is given to each bond and this number is kept fixed during the whole of the simulation (it represents the radius of the duct). At each step, the interface is moved to invade the bond adjacent to the interface, where the probability number is the largest (without invasion of the trapped clusters). A simulation of this mechanism on two-dimensional network (size 75×75) is shown in figure 13(*a*) (after Lenormand & Bories 1980). The heavy line shows the continuous path between the entrance and the exit. This pattern is similar to the result of the network simulator (figure 4*a*, $\log C = -10.7$) and the experiments in the capillary domain (figure 10*c*, Hg–A 4).

Invasion percolation is a 'local model', i.e. at each step, the injected fluid invades one pore (or site) according to the size of the throats along the frontier. At a given stage, menisci in the pores do not 'see' the exit because we are assuming a zero pressure drop in the fluids. The mechanism is different for viscous displacements.

6.2. *Viscous displacement and dielectric breakdown model*

Viscous displacements, either stable or unstable, are governed by the pressure field between the entrance and the exit. Consequently, even in the case of stable displacement, a local model based on some rules at the interface cannot be realistic. A model, called 'the Dielectric Breakdown Model' (DBM) (Niemeyer, Pietronero & Weismann 1984) has been adapted to solve viscous flow in porous media (see Sherwood 1987 for a review). This model uses a continuum approach to calculate the pressure field together with a discrete displacement of the interface which accounts (in some sense) for the granular structure of the porous medium.

Let us now examine the two extreme cases when $M \to 0$ and $M \to \infty$ for which the DBM can be replaced by two simpler models: diffusion-limited aggregation (DLA) and anti-DLA.

$M \to 0$: Diffusion-limited aggregation (DLA)

In this case, the pressure drop in the injected fluid is negligible and therefore the pressure field is only calculated in the displaced fluid. The patterns obtained in the viscous-fingering domain (figure 4*a*, $\log C = -5.7$) are similar to those obtained by the DLA model (Paterson 1984; Lenormand & Zarcone 1984*b*; Måløy, Feder & Jøssang 1985). DLA can be represented by the following process: a seed particle or a line is placed on a lattice and another particle, launched from far away, moves at

random and sticks when it reaches the seed or the line (Witten & Sander 1983). Another particle is launched and so forth. This diffusive process produces very ramified clusters, as shown in figure 13*b* (after Houi & Lenormand 1984), in the case of sticking on a line seed.

$M \to \infty$; anti-DLA

From computer simulations at high capillary number, we observe that trapping of very small clusters still occurs when $M \to \infty$ (figure 4*c*, $\log M = 2$), and that the displacement cannot be described by a flat interface. Paterson (1984) was the first author to suggest the relationship between a stable displacement in a porous medium and an *anti-DLA* process. More recently Meakin & Deutch (1986) have presented detailed properties of a similar model called *diffusion-limited annihilation*.

The anti-DLA model consists in releasing particles (equivalent to fluid 2) near a compact aggregate (the pore network filled by fluid 1 in our case). The particle moves at random until it reaches an occupied site. In this case, the particle and the site are removed and a new particle is released. Figure 13 (*c*) shows the result of an anti-DLA simulation on a 100×100 network, where we added a condition of non-annihilation on a disconnected cluster to take into account the trapping of the displaced fluid. The main result of Meakin & Deutch is that the asymptotic variance of the front thickness scales with the width L of the network according to $[\ln (L)]^{\frac{1}{2}}$.

6.3. *The phase-diagram and statistical models*

Although the analogy between viscous fingering and DLA or DBM has never been definitively assessed (Kadanoff 1985; Chan, Hughes & Patterson 1986), the similarity between the patterns is striking. So, we shall assume that each of the three main regimes of displacement of one fluid by another can be described by the following statistical models:

Viscous fingering simulated by diffusion limited aggregation (DLA) (or $M \to 0$ limit for DBM).

Stable displacement simulated by anti-DLA (or $M \to \infty$ limit for DBM).

Capillary fingering simulated by invasion percolation.

The next step will be the direct calculation of each of the boundaries of the diagram (lines A–F, figure 8) by using the statistical theories described above. Some results on the scaling laws in an 'infinite' porous medium by means of DLA and invasion percolation have been published (Lenormand 1986). However, the relationship between the pore size distribution and the randomness of the statistical models needs further studies (Chen & Wilkinson 1985; Nittmann & Stanley 1986).

At this point, can we answer the fundamental question about the relationship between these statistical models and the classical macroscopic approach? The classical approach is based on the Representative Elementary Volume (REV) concept (Bachmat & Bear 1986): the properties of the solid medium (porosity, permeability) and of the fluids (saturations, relative permeabilities, pressure, etc.) are defined within a volume (REV) that is small compared with the sample size. This means, for instance, that the blob size must be much smaller than the sample size. We have shown that a large number of blobs of fluid 1 remain trapped after displacement. From simulations and experiments, we can assume that the maximum size of the blobs is of the same order as the finger length during the displacement. Consequently, the classical approach is valid inside the anti-DLA domain (maximum blob size of the order of $(\log L)^{\frac{1}{2}}$) and depending on the sample size, inside a large stripe around this domain. Obviously, the classical approach is not valid in the DLA and percolation domains where the finger length is of the order of the sample size.

7. Conclusions

The first point is the good agreement between the computer simulations and the experiments in micromodels when both capillary and viscous forces are acting. This study shows that the two approaches are complementary and necessary. The micromodels are used to generate the microscopic rules of the simulator and to check the validity of the results at large scale. On the other hand, the reproducibility of the 'numerical experiments' allows the study of parameters (such as the final saturation) that are difficult to obtain in physical experiments. In addition, numerical experiments can be performed when physical experiments are impossible because of technical limitations (pressure, time), which is the case for the series at $\log C = 0$.

The second point concerns the notion of the phase-diagram. Both simulations and experiments show the existence of three main regimes: stable displacement, viscous fingering and capillary fingering, which can be mapped onto the viscosity ratio–capillary number plane.

Each of these main regimes can be described by a statistical model: anti-DLA, DLA and invasion percolation. Although the analogies have not yet been demonstrated, the similarities between the patterns are striking. These statistical models and their cross-overs in transition zones will lead to general calculations of the boundaries of the phase-diagram.

This work has benefited from many conversations with Y. Pomeau and with colleagues at Schlumberger Doll Research (Ridgefield) and at Dowell Schlumberger (Saint Etienne). We also thank Y. Lardin who assisted with the experimental work and J. Sherwood for helpful criticisms of the manuscript. This research has been partially supported by C.N.R.S. (A.T.P. Milieux Aléatoires Macroscopiques).

REFERENCES

Bachmat, Y. & Bear, J. 1986 Macroscopic modeling of transport phenomena in porous media. 1: The continuum approach. *Transp. Por. Med.* **1**, 213–240.

Chan, D. Y. C., Hughes, B. D. & Paterson, L. 1986 Fluctuations, viscous fingering, and diffusion-limited aggregation. *Phys. Rev.* **A 34**, 4079–4082.

Chen, J. D. & Wilkinson, D. 1985 Pore-scale viscous fingering in porous media. *Phys. Rev. Lett.* **55**, 1892–1895.

Dias, M. M. & Payatakes, A. C. 1986*a* Network models for two-phase flow in porous media. Part 1. Immiscible microdisplacement of non-wetting fluids. *J. Fluid Mech.* **164**, 305–336.

Dias, M. M. & Payatakes, A. C. 1986*b* Network models for two-phase flow in porous media. Part 2. Motion of oil ganglia. *J. Fluid Mech.* **164**, 337–358.

Houi, D. & Lenormand, R. 1984 Particle deposition on a filter medium. In *Kinetics of Aggregation and Gelation* (ed. F. Family & D. P. Landau), pp. 173–176. Elsevier.

Kadanoff, L. P. 1985 Simulating hydrodynamics: a pedestrian model. *J. Stat. Phys.* **39**, 267–283.

Koplik, J. & Lasseter, T. J. 1985 One and two-phase flow in network models of porous media. *Chem. Engng Commun.* **26**, 285–295.

Lenormand, R. 1985 Différents mécanismes de déplacements visqueux et capillaires en milieu poreux: Diagramme de phase. *C.R. Acad. Sci. Paris II* **301**, 247–250.

Lenormand, R. 1986 Scaling laws for immiscible displacements with capillary and viscous fingering. *SPE* 15390 *61th Annual Tech. Conf. and Exhib. of SPE, New Orleans, La, Oct.* 5–8.

Lenormand, R. & Bories, S. 1980 Description d'un mécanisme de connexion de liaisons destiné à l'étude du drainage avec piégeage en milieu poreux. *C.R. Acad. Sci. Paris* **291 B**, 279–280.

LENORMAND, R. & ZARCONE, C. 1984*a* Role of roughness and edges during imbibition in square capillaries. *SPE* 13264, *59th Annual Tech. Conf. and Exhib. of SPE, Houston, Texas, Sept. 16–19.*

LENORMAND, R. & ZARCONE, C. 1984*b* Two-phase flow experiments in a two-dimensional permeable medium. *Proc. Physiochemical Hydrodynamics 5th International Conference, Tel-Aviv*; *Phys. Chem. Hydrodyn.* **6**, 497–506, 1985.

LENORMAND, R., ZARCONE, C. & SARR, A. 1983 Mechanisms of the displacement of one fluid by another in a network of capillary ducts. *J. Fluid Mech.* **135**, 337–353.

MÅLØY, K. J., FEDER, J. & JØSSANG, T. 1985 Viscous fingering fractals in porous media. *Phys. Rev. Lett.* **55**, 1885–1891.

MEAKIN, P. & DEUTCH, J. M. 1986 The formation of surfaces by diffusion limited annihilation. *J. Chem. Phys.* **85**, 2320–2325.

NIEMEYER, L., PIETRONERO, L. & WIESMANN, H. J. 1984 Fractal dimension of dielectric breakdown. *Phys. Rev. Lett.* **52**, 1033–1036.

NITTMANN, J. & STANLEY, H. E. 1986 Tip splitting without interfacial tension and dendritic growth patterns arising from molecular anisotropy. *Nature* **321**, 663–668.

PATERSON, L. 1984 Diffusion-limited aggregation and two-fluid displacements in porous media. *Phys. Rev. Lett.* **52**, 1621–1624.

SHERWOOD, J. D. 1987 Unstable fronts in a porous medium. *J. Comp. Phys.* **68**, 485–500.

WILKINSON, D. 1985 Multiphase flow in porous media. In *Physics of Finely Divided Matter* (ed. N. Boccara & M. Daoud), pp. 280–288. Springer.

WITTEN, T. A. & SANDER, L. M. 1983 Diffusion limited aggregation. *Phys. Rev.* **B27**, 5686–5697.